Evidence of spatial periodic firing in the subiculum of mice

P. Abad-Perez[1, 2 ,3 ∞], G. Rigamonti[1,2,3∞] , F.J. Molina-Paya, G. Cabral-Pereira[2], M. Esteve[1], R. Scott [4], V. Borrell [2,3], L. Martínez-Otero [2,3] , A. Falco[1], J.R. Brotons-Mas[12,3]*

[1] *Universidad Cardenal Herrera-CEU, CEU Universities, Spain*

[2] *Instituto de Neurociencias UMH-CSIC. Alicante*

[3] *Grupo de Investigación Multidisciplinar en la enfermedad de Alzheimer UMH-UCHCEU*

[4] *Universidad de Alicante, Alicante*

[∞] Pablo Abad -Pérez and Giulia Rigamonti equally contributed to this work and appear in alphabetical order.

* Corresponding author: Jorge R Brotons-Mas

e-mail: jorge.brotonsmas@uchceu.es; jbrotons@umh.es

Address: Universidad CEU Cardenal Herrera; Plaza Reyes Católicos, 19. 03204 Elche Alicante, Spain

Instituto de Neurociencias UMH-CSIC; Avd Ramón y Cajal SN, Edificio Ramón y Cajal, 03550,San Juan de Alicante, Alicante, Spain.

Abstract

The subiculum is a critical node of the hippocampal formation, integrating multiple circuits—including thalamic inputs and afferents from CA1 and medial entorhinal cortex—and projecting broadly to cortical and subcortical targets. Yet its contribution to spatial coding remains incompletely understood. We recorded single units in freely moving mice using two complementary approaches: (i) chronic tetrodes targeting CA1 and dorsal SUB, and (ii) 64-channel linear silicon probes targeting dorsal SUB. In addition to place cells, boundary-vector cells (BVC) and corner cells (CC), we identified a subset of SUB neurons that exhibited spatially periodic (grid-like) firing. This phenomenon was replicated across recording technologies indicating that periodic coding is a consistent feature of mouse subiculum. Compared with CA1 place cells, SUB spatial neurons showed lower spatial information and reduced within-session stability, suggesting distinct coding regimes across these hippocampal subregions. Sampling along the proximodistal axis with probe arrays further revealed that burst propensity correlated positively with spatial information at more distal recording sites, consistent with known physiological gradients in subiculum and echoing relationships seen in CA1. Together, these results expand the repertoire of identified spatial codes in SUB and support a view in which subiculum contributes to geometry- and periodicity-based representations that complement CA1 and entorhinal spatial representation, thus, shaping downstream computations in cortico-subcortical circuits.

Keywords:

Subiculum; spatial coding; grid-like firing; place cells; boundary-vector cells; corner cells; bursting; proximodistal gradient; silicon probes; tetrodes.

Significance Statement:

Spatial information and memory emerge from interactions among hippocampal and entorhinal circuits with diverse, spatially tuned neurons. Here we provide the first evidence in mice that pyramidal neurons in the subiculum exhibit grid-like, spatially periodic firing, replicated across tetrodes and high-density probes. These findings suggest that the subiculum contributes to computations beyond simple relay/integration of CA1 inputs, adding a periodic component to subicular spatial coding that may shape downstream cortico-subcortical circuits.

Introduction

Since the discovery of hippocampal place cells, neurons that code for space by being active in specific locations of the environment (1), multiple efforts have aimed to understand the computational bases of spatial navigation. As a result, different types of spatially modulated neurons have been described across brain regions: head direction cells (HD); border and boundary vector cells (BVC), coding for the geometry of the environment in medial entorhinal cortex (MEC) and the SUB; and grid cells (GC) in the medial entorhinal cortex (MEC) (2–8). These neurons are either strongly involved in the codification of external information, such as BVC coding for geometry, or in egocentric related information. This is the case for grid cells (GC), where tessellating regular firing is associated with the representation of spatial metrics and is therefore essential for path integration—the ability to navigate in the absence of external cues (9). The integration of both allocentric and egocentric streams of information is instrumental in generating an efficient spatial representation.

Multiple computational models have sought to uncover the mechanisms underlying the integration of different types of spatial signals. The BVC model suggested that place cells require the existence of neurons coding for the geometry of the environment (10). Other models suggested that place cells require GC activity (2,11). However, single unit recordings during neurodevelopment demonstrated that HD, place cells and boundary neurons appear before GC during neurodevelopment (12,13). Thus, the dependence of place cells activity on grid cell firing seems to be unclear (14) .

Further research has considered the heterogeneity among different spatial cell types and their distributed anatomical localizations. In this context, the SUB may serve as a critical anatomical hub for spatial navigation (15,16). Strategically located between the EC and CA1, the SUB supports spatial information processing in a complex and heterogeneous manner. While spatial neurons in CA1 typically exhibit spatial reliability, the behavioral

correlates of SUB neuron activity include location, speed, direction, and the geometry of the spatial context, while also providing a reliable representation of space across light-dark transitions (17–20). The SUB contains neurons with a diverse electrophysiological characteristic that might have different roles in memory processing (21,22).

Previous work in rats indicated the existence of grid-like, spatially tuned activity in the SUB, attributed to axonal inputs from the MEC (8). This raised the possibility that SUB pyramidal neurons could integrate periodic signals from the EC and aperiodic signals from CA1. However, whether such grid-like activity originates from local SUB pyramidal neurons has not been extensively investigated until now. Here, we sought to test the presence of periodic firing in individual SUB cells of mice using large open-field arenas. We found evidence of grid-like and other forms of spatially periodic firing (i.e., band-like,(23) in SUB neurons whose electrophysiological characteristics are compatible with pyramidal neurons**.** To the best of our knowledge, this is the first evidence of spatially periodic neurons in the mice SUB, highlighting the potential role of this structure in shaping the spatial cognitive map.

Methods

Subjects

Male wild-type C57BL/6 mice, N=11, age p60 to p90 supplied by the UMH “Servicio de Experimentación Animal (SEA)" were used. Mice were maintained on a 12 h light/dark cycle with food and water available *ad libitum* and were individually housed after electrode implantation. All procedures were approved by the UMH-CSIC ethics committee, and the regional government, and they complied with local and European guidelines for animal experimentation (86/609/EEC).

In vivo recordings on freely moving mice.

Custom-designed microdrives (Axona Ltd.) carrying twisted-wire tetrodes (12 μm tungsten; California Fine Wire, Grover Beach, CA, USA) targeted dorsal CA1 and dorsal subiculum. Under isoflurane anesthesia (1.5%) with peri-operative buprenorphine (0.05 mg/kg, s.c.), small craniotomies were made over dorsal hippocampus and dorsal subiculum. Guide cannulas were aimed at dorsal CA1 (AP −2.2 mm, ML +1.0 mm from bregma) and predominantly proximal dorsal subiculum (AP −2.7 mm, ML +0.5 mm; right hemisphere; Fig. 1A). Of the animals implanted with microdrives, three met anatomical/physiological criteria for inclusion in both CA1 and SUB datasets. Because tetrodes advance along a single guide, coverage along the proximodistal axis was limited. To increase yield and proximodistal coverage, and the number or recorded neurons, a separate cohort of two mice was implanted with 64-channel linear silicon probes (NeuroNexus, Ann Arbor, MI, USA) targeting dorsal subiculum (AP −3.8 mm, ML +1.5 mm), coordinates chosen to maximize subicular coverage. The linear arrays (≈800 μm span) enabled sampling from proximal to more distal positions within dorsal subiculum. Electrode depths (tetrodes and probes) were adjusted across days until characteristic hippocampal/subicular activity was observed.

Data acquisition.

Tetrode recordings. As in our prior work (24) recordings were obtained using 16-channel headstage (gain x1), with an infrared light-emitting diode (LED) to track mouse position (Axona Ltd, UK). Signals were amplified (400 to 1000x), band pass filtered 0.3 Hz to 24 KHz, (Dacq system, Axona, UK) and recorded at 48 KHz/24 bit precision.. For single unit recordings, the signal was band-pass filtered between 380 Hz and 6 KHz. Spikes were recorded whenever the signal was 3-4 times above background noise, typically 20-30 μV, and stored in windows of 1 ms duration (200 ms before threshold and 800 ms after threshold detection). Spike waveforms were sampled at 48 KHz while the same channels were also recorded in continuous mode at 4.8 KHz and band-pass filtered between 0-3-2.4 KHz.

Silicon-probe recordings. In line with our earlier work (25), high-density recordings were obtained with an Intan-based system (NeuroNexus, Ann Arbor, MI, USA) at 30 kHz / 16-bit. The wideband stream was used for spike sorting; a downsampled 1.25 kHz copy served as the LFP signal. During sessions, electrode advancement and target verification relied on electrophysiological landmarks—ripple power, unit activity, and theta power—to optimize depth and confirm subicular/hippocampal placement.

Place cells recordings.

Mice performed a pellet-chasing task. Animals were maintained under mild food restriction (≤20% below free-feeding weight). During recording, small food pellets were tossed pseudo-randomly into the arena at ~20s intervals to sustain locomotion and promote uniform spatial sampling. All mice were habituated to each arena for several days before recording. Tetrode-implanted mice were recorded in a 50 × 50 cm arena (20 min) and in a larger 70 × 70 cm arena (30 min). The silicon-probe cohort was recorded in an 80 × 80 cm arena (30–40 min) to maximize the chances of detecting grid/periodic firing.

Data Analysis.

Local field potential data was analyzed using custom-written MatLab codes (Mathworks, Natick, MA, USA). Raw recordings were FIR filtered (<1.2 KHz) and down sample to 2.4 KHz. Similar to previous studies (24,26), data obtained from open-field recordings was used to characterize the LFP. To visualize the power spectrum in relationship to the speed of movement, the spectral power (in decibels, 10log10) and spectrogram was built using the Thomson multi-taper method. A sliding window with 50% overlap, yielding a frequency resolution of 1 Hz was used.

Unit isolation and spike train analysis.

Single-unit activity from tetrode recordings was isolated with TINT (Axona, St. Albans, UK). This software is specifically designed for tetrode data cluster sorting. Feature vectors included the first principal components, peak-to-trough duration, peak and trough amplitudes, time of peak and trough, and waveform energy on each wire. KlustaKwik was used for initial automated clustering, followed by manual curation in TINT based on principal components, spike amplitude, and waveform consistency. Cluster quality was quantified by the overlap probability metric as described previously (24,27). Spike trains were analyzed by generating interval time histograms and temporal auto-correlogram. Only units with no spikes in the refractory period of the inter-spike time histogram (1-2 ms), and with spike amplitudes 3-4 times above background noise, typically 20-30 mV, were included. Putative pyramidal cells and interneurons were distinguished based on waveform duration and firing rate characteristics, as previously described (8). Further spike train analysis was performed to determine the bursting properties of the recorded neurons using the burst index (BI) proposed by Royer and the propensity to burst (PrtB) proposed by Staff (28,29).

For high-density recordings with silicone probes we followed the same approach as in our previous work (25). In brief, spike sorting was performed semi-automatically with KiloSort (https://github.com/cortex-lab/KiloSort) via the KilosortWrapper pipeline

171 (https://github.com/brendonw1/KilosortWrapper), as in (9, 10, 56). Resulting clusters
172 were manually refined in Phy (https://github.com/kwikteam/phy) using community plug-
173 ins (https://github.com/petersenpeter/phy2-plugins). The following parameters were
174 used for KiloSort: pos.Nfilt: 6 *numberChannels; ops.nt0: 64; ops.whitening: 'fulll';
175 ops.nSkipCov: 1; ops.whiteningRange: 64; ops.criterionNoiseChannels: 0.00001;
176 ops.Nrank: 3; ops.nfullpasses: 6; ops.maxFR: 20000; ops.fshigh:300; ops.ntbuff: 64;
177 ops.scaleproc: 200; ops.Th: [4 10 10]; ops.lam: [5 20 20]; ops.nannealpasses: 4;
178 ops.momentum: 1./[20 800]; ops.shufflеclusters: 1. Electrophysiological neuron
179 classification was performed using CellExplorer (https://cellexplorer.org) (Petersen et al.,
180 2021). This algorithm classifies units using two main features: spike waveform width
181 (trough-to-peak, TTP) and burstiness derived from the autocorrelogram (ACG). Using
182 the waveform and burstiness criteria, units are tentatively segregated to narrow
183 waveform (trough-to-peak ≤ 450 μs), wide waveform (trough-to-peak > 450 μs and τ_{rise} >
184 6 ms), putative interneurons, and the rest, pyramidal neurons or unclassified. Because
185 tetrode spikes were extracted from thresholded high-pass snippets whereas probe
186 spikes were extracted from broadband continuous data, we did not compare absolute
187 waveform amplitudes across technologies. All downstream spatial metrics (rate-map
188 construction, information, coherence, stability) and grid/periodicity analyses were
189 identical for tetrode and probe datasets.

190 Phase locking to ongoing oscillations

191 Phase locking of single units to ongoing oscillations was computed as previously
192 described (25,30). The analysis toolbox is available online
193 (https://github.com/valegarman/HippoCookBook). The LFP was filtered for each
194 frequency of interest, and the Hilbert transform was applied to obtain the instantaneous
195 phase. Phase locking was computed by calculating the phase angles for each timestamp
196 where an action potential occurred. A histogram of phase angles was calculated, and
197 the circular mean and resultant vector were calculated for each neuron (31). Only

neurons that were significantly modulated (Rayleigh test) for each frequency band during the baseline condition were included for the analysis.

Firing rate maps

In the case of the tetrode recordings, firing-rate maps were assembled as described previously (8,32). Pixel maps were converted to a bin matrix with a bin size of 2.5 cm x 2.5 cm. Firing rate in each bin was determined by a smoothing process using overlapping squares of 7.5 cm x 7.5 cm, as described before. Firing fields were plotted as a contour map reflecting the frequency of firing; colors were interpolated from the top firing bins down to the lowest firing areas by scaling them in decreasing intervals of the peak firing and giving them a color scale: red highest frequency, dark blue, lowest frequency. A similar approach was implemented with multisite experiments, however, in this case the FMA toolbox was used (https://fmatoolbox.sourceforge.net/.).

For both sets of data, the spatial information content per spike and per second was quantified using the Skaggs information indexes for the smoothed map (33) . In addition, spatial coherence, a spatial autocorrelation measurement**,** was calculated as the correlation coefficient between the firing rate of each bin and the average rate of its eight surrounding bins (34). Firing fields were defined as a group of 6 contiguous bins, where the firing frequency was above the mean firing frequency plus the standard error of the firing matrix. The maximal firing frequency of this group of bins had to be above 1 Hz. For those units displaying more than one firing field, firing field size was computed as the sum of the existing firing fields and expressed as the percentage of the arena size occupied by the firing field calculated using the smoothed firing matrix. In-field maximum frequency was computed as the maximum firing field frequency of the smoothed firing map. Mean frequency was computed as the total number of spikes divided by the total recording time to provide the average session firing rate expressed in Hz.

To classify units as having spatially related activity, a randomized distribution was calculated by circular shifting the spikes times vs the position. This strategy allowed us to generate a random distribution without affecting the temporal firing structure of neurons (13). The values were obtained from the original unsmoothed firing map while respecting the original trajectory of mice (n=1000). For a unit to be regarded as being spatially modulated, it had to display a spatial coherence above 95% of the randomized distribution. This same random distribution was used to obtain the intratrial stability index between the original and a random distribution. Thus, for units to be regarded as stable they had to be above the 95% of cross-correlation between the original and the randomized distribution.

Spatial typology analysis

Multiple spatial response types have been reported in subiculum (8,35,36). Here we specifically tested periodic (grid-like) firing and distinguished it from boundary-vector cells (BVCs), corner cells (CCs), and place cells (PCs) using the procedures below.

Grid analyses and periodic firing analyses.

Grid analyses were implemented following similar criteria to previous studies (2). Spatial autocorrelograms were calculated for each firing map.

$$r(\tau_x,\tau_y)=\frac{n\sum\lambda(x,y)\lambda(x-\tau_x,y-\tau_y)-\sum\lambda(x,y)\sum\lambda(x,y)\sum\lambda(x-\tau_x,y-\tau_y)}{\sqrt{n\sum\lambda(x,y)^2-(\sum\lambda(x,y))^2}\sqrt{n\sum\lambda(x-\tau_x,y-\tau_y)^2-(\sum\lambda(x-\tau_x,y-\tau_y))^2}}$$

where r is the autocorrelation between the original firing rate map and its spatially shifted copy. The lag τ is normally 1-dimensional for signal analysis. Because of the 2-dimensional nature of the firing rate map, the autocorrelation has lags in the x- and y-directions: τx and τy. n is equal to the number of pixels. To determine the existence of a hexagonal grid firing structure, grid index, size and orientation were calculated as described previously (8,37).

247 To obtain the “gridness index” we obtained a circular portion of the spatial
248 autocorrelogram generated from the spatial firing matrix. This circle was centered on the
249 central peak which was eliminated from the matrix. Then we correlated the rotated
250 versions, in steps of 6º , of this matrix with the original spatial autocorrelogram. The
251 degree of spatial periodicity (gridness’ or ‘grid scores’) was determined for each recorded
252 cell and the grid index calculated as previously described (37,38).

253 Additionally, to further investigate the presence of periodic firing we obtained the sum of
254 values of the 2D resulting map in all its orientation and we displayed the preferred
255 orientation of these neurons in space as a polar plot (23). These values were plotted
256 against the polar plot of the shuffled original firing map, n=1000. Only neurons that
257 showed higher values than this confidence interval were considered as periodic neurons.

258 **Boundary vector cells (BVC) and Corner cells (CC)**

259 To identify BVC we follow the same methodology as previously described (39). This
260 analysis implied the comparison of the original map with idealized BVC. Spatial shuffling
261 was performed as described above. Model BVCs were fit to these spatially shuffled rate
262 maps as described above. To be classified as a BVC, the $r_{(max)}$ value for each cell had to
263 surpass the 95th percentile of the 1000 shuffled $r_{(max)}$ values generated for that specific
264 cell and trial while meeting the same criteria to be spatially modulated.

265 Corner cells were identified following the same procedure as described by Sun et al,
266 (36). Field location was taken as the regional maximum (x,y) of each region. Centroid
267 and corner coordinates were detected manually verified. For each field we computed a
268 corner score

269 $$\boldsymbol{corner\ score} = (\boldsymbol{d1} - \boldsymbol{d2})/(\boldsymbol{d1} + \boldsymbol{d2})$$

270 Where *d1* is the distance from the field maximum to the environment centroid and *d2* is
271 the distance to the nearest corner. The score ranges from **−1** (centroid) to **+1** (ideal

272 corner). The total corner score of the cell was calculated as the mean of the corner
273 scores of the firing fields and that we considered corner cell only if the total index was
274 above 95th of the shuffling distribution in addition the neuron had more than one firing
275 field. Units that did not meet GC, BVC or CC were deemed as place cells (PC).

276 Histological Analysis

277 After completing experiments, animals were sacrificed using sodium pentobarbital (180
278 mg/kg at a concentration of 100 mg/ml) and transcardially perfused with saline and 4%
279 paraformaldehyde. This procedure was authorized by the ethical commission according
280 to the current normative and following veterinary recommendations. The brains were
281 removed, sliced in 40 µm sections, and prepared for immunohistochemistry. For primary
282 antibodies we used anti-NeuN (anti-NeuN 1:500; Millipore #MAB377) and GFAP (Merck,
283 SAB2500462-100UG; host: goat; dilution 1:1000), and for secondary Anti-goat,
284 (Invitrogen, A11055; dilution 1:1000) for electrode localization. Nuclei were stained with
285 DAPI (Sigma-Aldrich, D9542-10ML). Electrode tracks were identified when visible and
286 their position estimated by comparison with anatomical landmarks using the Paxinos and
287 Franklin stereotaxic atlas. In addition, the presence of local electrophysiological
288 signatures (e.g., ripple activity, theta oscillations) provided further confirmation of
289 electrode placement. In those cases where a clear electrode track was not detectable,
290 the location of the electrodes was inferred based on implant coordinates, electrode
291 design, and characteristic electrophysiological landmarks.

292 Statistical analysis

293 Distribution of dependent variables was tested for normality and for equal variance.
294 Parametric statistical tests were used for normally distributed variables and non-
295 parametric tests were used for variables that did not show normal distribution. All
296 descriptive values are expressed as mean ± the standard error (S.E.). Statistical
297 significance was set at $p < 0.05$. All statistical analysis was performed using SPSS (IBM,
298 V27) software package and MATLAB statistic toolbox, (Mathworks, Natick, MA, USA).

Results

Tetrode recordings in the CA1 and SUB

To test for spatially periodic cells in subiculum, we recorded in standard (50 × 50 cm) and large (70 × 70 cm) open fields. Across eight mice (five implanted in CA1, one in SUB, and three in both regions), histology confirmed the placement of three tetrodes in three different mice in the SUB (Fig. 1A-B) we recorded 147 CA1 and 65 SUB neurons. Units were classified by spike duration, waveform shape, and firing rate (Fig. 1C), following established criteria (7). Of these, 74 CA1 and 28 SUB cells met pyramidal and spatial-modulation criteria (Methods).

Unit isolation quality did not differ between regions (CA1 vs. SUB overlap probability: 0.06 ± 0.01 vs 0.10 ± 0.02; Mann–Whitney U = 4290, p = 0.236), like previous reports (24,27). Spike amplitude and duration were also similar (duration: 477.5 ± 7.8 μs vs 491.0 ± 10.4 μs, U = 862, p = 0.192; amplitude: 254.1 ± 11.9 μV vs 226.1 ± 15.6 μV, U = 943, p = 0.48; Fig. 1C–). In contrast, SUB neurons fired faster than CA1 neurons (mean rate: 1.8 ± 0.2 Hz vs 1.2 ± 0.12 Hz; U = 745, p = 0.02; Fig. 1F), consistent with prior reports (7,18,40).

The interaction between the CA1 and the SUB is critical for the organization of inputs and outputs of the hippocampal formation. This dialog depends on the specific timing of the activity of different populations of neurons in different theta cycle windows (41). Therefore, examining the relationship between CA1 and SUB firing and local LFP is fundamental to understanding the temporal dynamics of the hippocampal formation. We investigated the relationship between the firing of CA1 and SUB neurons with the locally recorded theta (4-12Hz). To target the pyramidal cell layer, we selected tetrodes on which ripples showed no slow (positive or negative) component, a standard indicator of pyramidal-layer placement. In CA1, preferred firing phases were bimodally distributed, with units clustering around the ascending and descending phases of the local theta

cycle and an additional concentration near the trough (Fig. 1F). For subiculum, we applied the same tetrode-selection criterion and computed phase from the local LFP on the same tetrode; subicular neurons preferentially fired near the theta peak in the tetrode database (Fig. 1G).

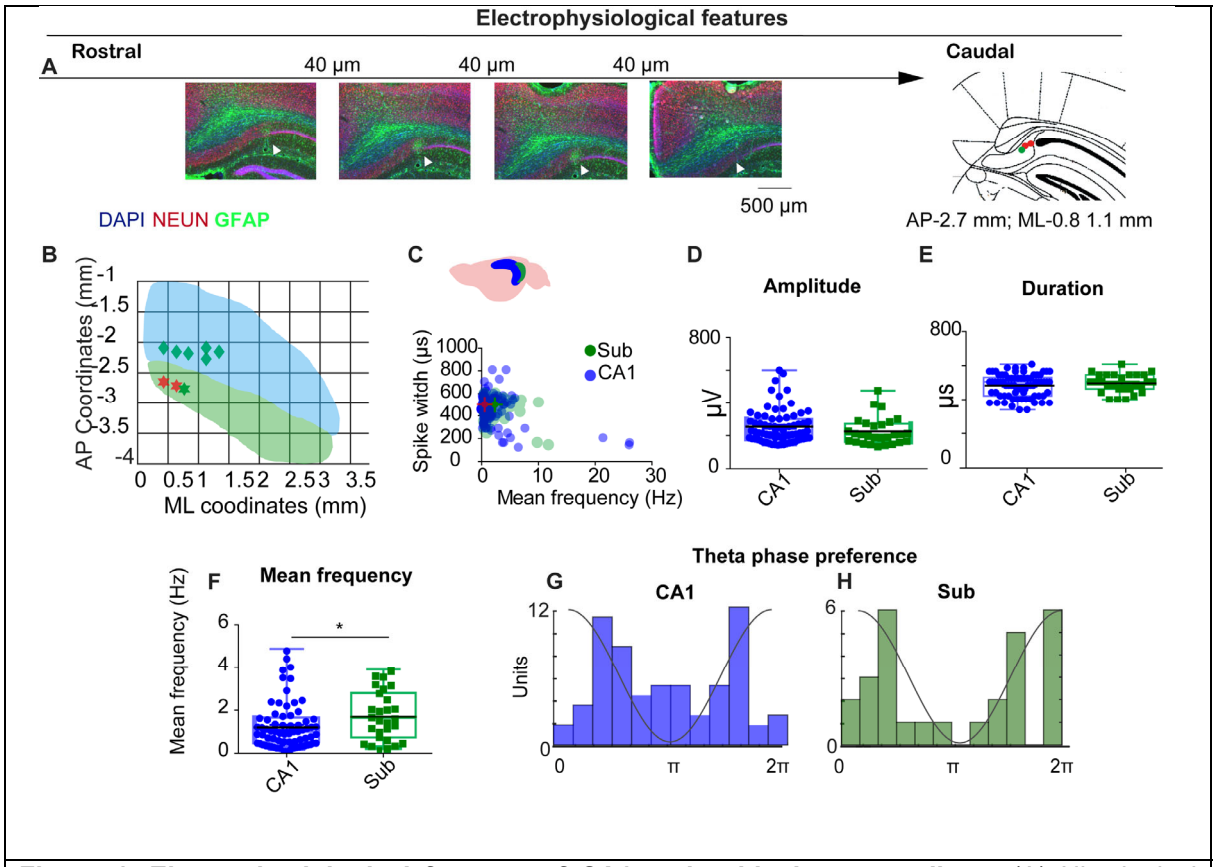

Figure 1. Electrophysiological features of CA1 and subiculum recordings. (A) Histological verification of tetrode tracks across the rostro-caudal extent of dorsal subiculum (DAPI/NEUN/GFAP). Arrowheads, electrode tip; schematic at right shows example target (AP −2.7 mm; ML +0.8–1.1 mm). Scale bars as indicated. (B) Recording coverage in mediolateral (ML) and anteroposterior (AP) coordinates; green = SUB, blue = CA1. (C) Scatter of spike width (trough-to-peak, µs) vs mean firing rate (Hz) for CA1 (blue) and SUB (green). (D–F) Group comparisons for spike amplitude (D), spike duration (E) and mean firing rate (F). SUB neurons fired faster than CA1 (see Results). (G–H) Theta phase preference histograms (4–12 Hz) for CA1 (G) and SUB (H); CA1 shows bimodality with a concentration near trough; SUB preferentially fires near the theta peak.

A group of subicular neurons showed grid and spatially periodic firing

In rats, subicular spatial coding comprises a heterogeneous mix of place cells (PC) and boundary-vector cells (BVCs), as well as corner cells (CC) (5,8,36). Given the larger body size of rats relative to typical arena dimensions, spatial periodicity may have been difficult to detect. In mice recorded in 50 × 50 cm arenas, we observed that several SUB neurons exhibited spatial periodic firing resembling grid-like structure. In contrast to prior reports (8), these units had pyramidal-like waveforms, were stable within session, and were well

338 isolated (Fig. 2A–D). Their spatial firing showed hexagonal periodicity by both
339 autocorrelogram and frequency-domain analyses (Fig. 2E–G). CA1 pyramidal neurons
340 recorded in the same arenas did not show comparable periodic patterns (Fig. 2H–N).
341 Overall, 4 of 28 spatially modulated SUB units (14%) met our gridness criterion (three
342 cells in one mouse and one cell in a second mouse).

343 To test the robustness of subicular periodicity across scales, we tracked individual SUB
344 neurons across 50 × 50 cm and 70 × 70 cm boxes. Some cells deviated from perfect
345 hexagonal symmetry in the larger arena yet retained clear periodic structure, similar to
346 observations in MEC under certain conditions (23). Fig. 3A–E vs. 3A′–E′). Conversely,
347 we identified at least one cell that showed a single dominant place field in the 50 × 50
348 cm arena but developed periodic firing in the 70 × 70 cm arena, as revealed by the 2D
349 FFT and related metrics (Fig. 3F–J vs. 3F′–G′).

350

351

352

353

354

355

356

357

358

359

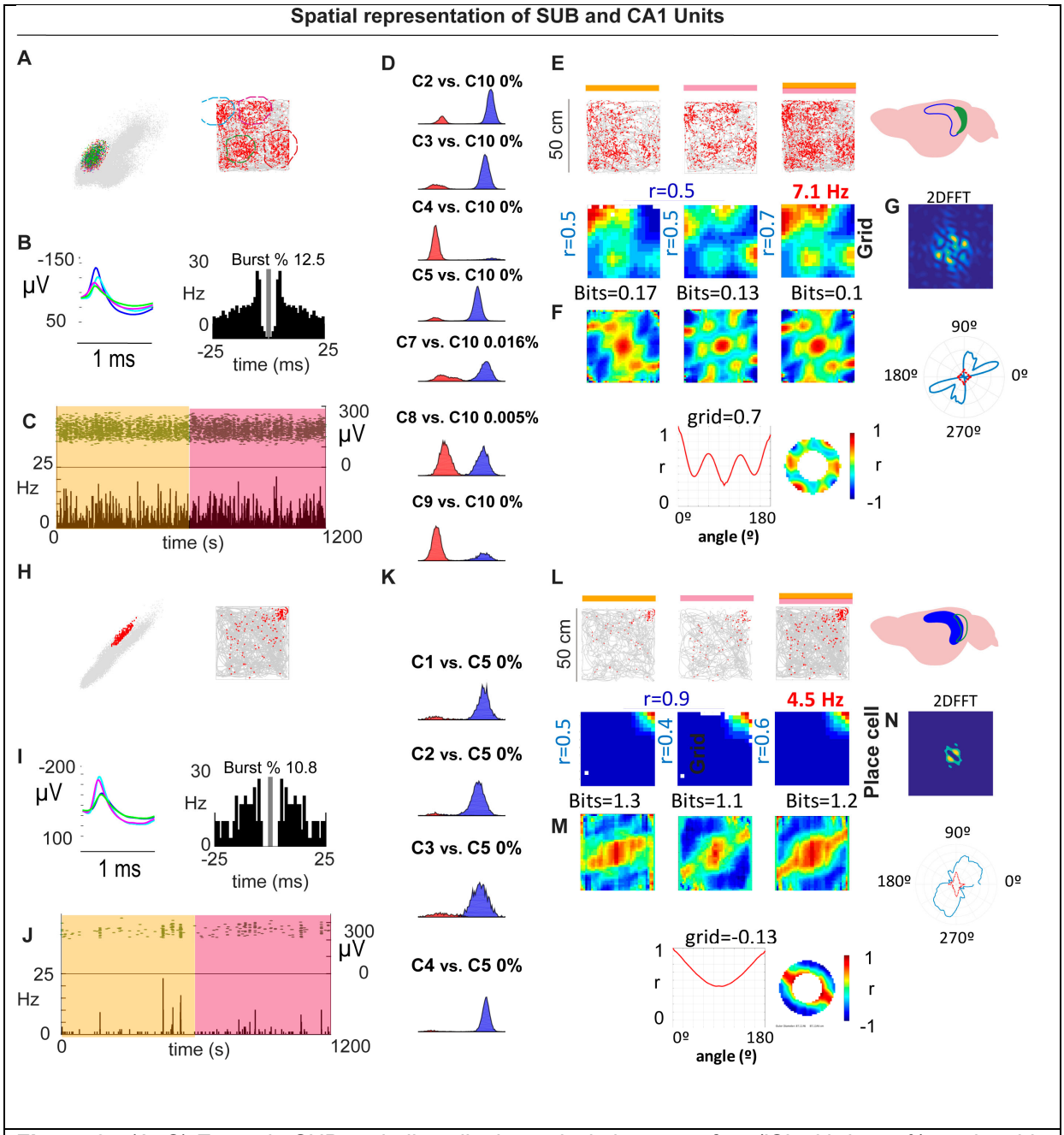

Figure 2. (A–C) Example SUB periodic cell: cluster isolation, waveform/ISI with burst %, and stable firing across the session.(D) Overlap probability controls for isolation quality (example comparisons). (E–F) Rate maps and autocorrelograms across spatial bins with corresponding gridness/periodicity summaries and 2D FFT (G). (H–J) Example CA1 place cell recorded in the same arena: isolation (K), rate maps/autocorrelograms (L, M) and 2D FFT (N). CA1 pyramidal units did not exhibit periodic/grid signatures under these conditions.

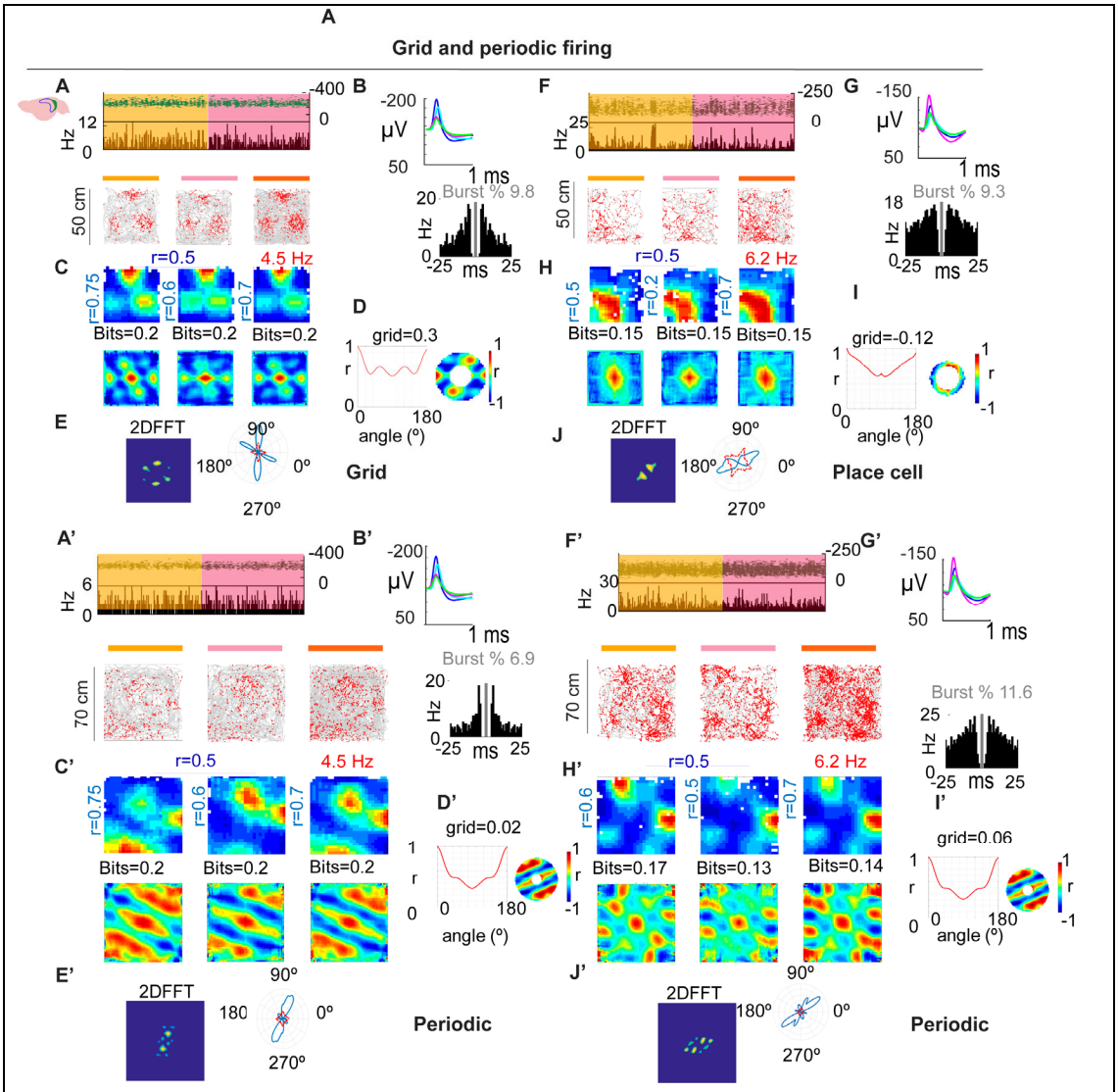

Figure 3. **Grid and spatially periodic firing across arena size.** (A–D) Example SUB neuron in 50 × 50 cm: stable firing (A), waveforms/ISI (B), rate maps and autocorrelograms (C), grid/periodicity summary (D) with 2D FFT (E). (A′–E′) Same neuron in 70 × 70 cm: periodic structure persists but deviates from perfect hexagonal symmetry (see main text). (F–J, F′–J′) Second example showing a place-like pattern in the small arena (G) that becomes periodic in the large arena, as confirmed by the 2D FFT (J, J′).

Spatial firing of SUB neurons showed lower spatial modulation than CA1

Spatial coding differs across hippocampal subregions (19,42). We compared CA1 and SUB using standard metrics spatial information per second, spatial information per spike, spatial coherence, and firing-field size. We found significant differences between CA1 and SUB neurons for the spatial information per second, spatial information per spike,

367 and for the spatial coherence, consistent with previous reports (Fig.4 A-C). In contrast,
368 (Fig. 4D), no significant differences were observed for the firing field size (CA1 vs SUB :
369 bits/s 0.39 ± 0.01 vs. 0.322 ± 0.06 μs,: U=738.0, p=0.025; bits/spike 0.43 ± 0.04 vs. 0.32
370 ± 0.06: U=611.0, p=0.001, Mann-Whitney; spatial coherence: (r), 0.61 ± 0.01 vs. 0.54 ±
371 0.02: $t_{(100)=}$2.442, p=0.016; firing field size (%), 29.02 ± 0.7 vs. 30.0 ± 1.14, $t_{(100)=}$-0.634,
372 p=0.528).

373 Because temporal instability can mimic rate remapping and obscure periodicity (43) we
374 assessed within-session stability by splitting each session into two 10-min halves, (Fig
375 4E) and computing bin-by-bin spatial correlations. We found that spatially periodic
376 signals that place cells in the CA1 region showed significantly higher spatial consistency
377 (CA1 vs SUB: intra trial stability coherence (r), 0.72±0.02 vs. 0.61±0.04: U=764.0,
378 p=0.041, Mann-Whitney). However, periodic neurons showed high stability within each
379 trial, (See Fig 3 for different examples), ruling out remapping effects as a confounding
380 factor in the identification of spatially-periodic firing.

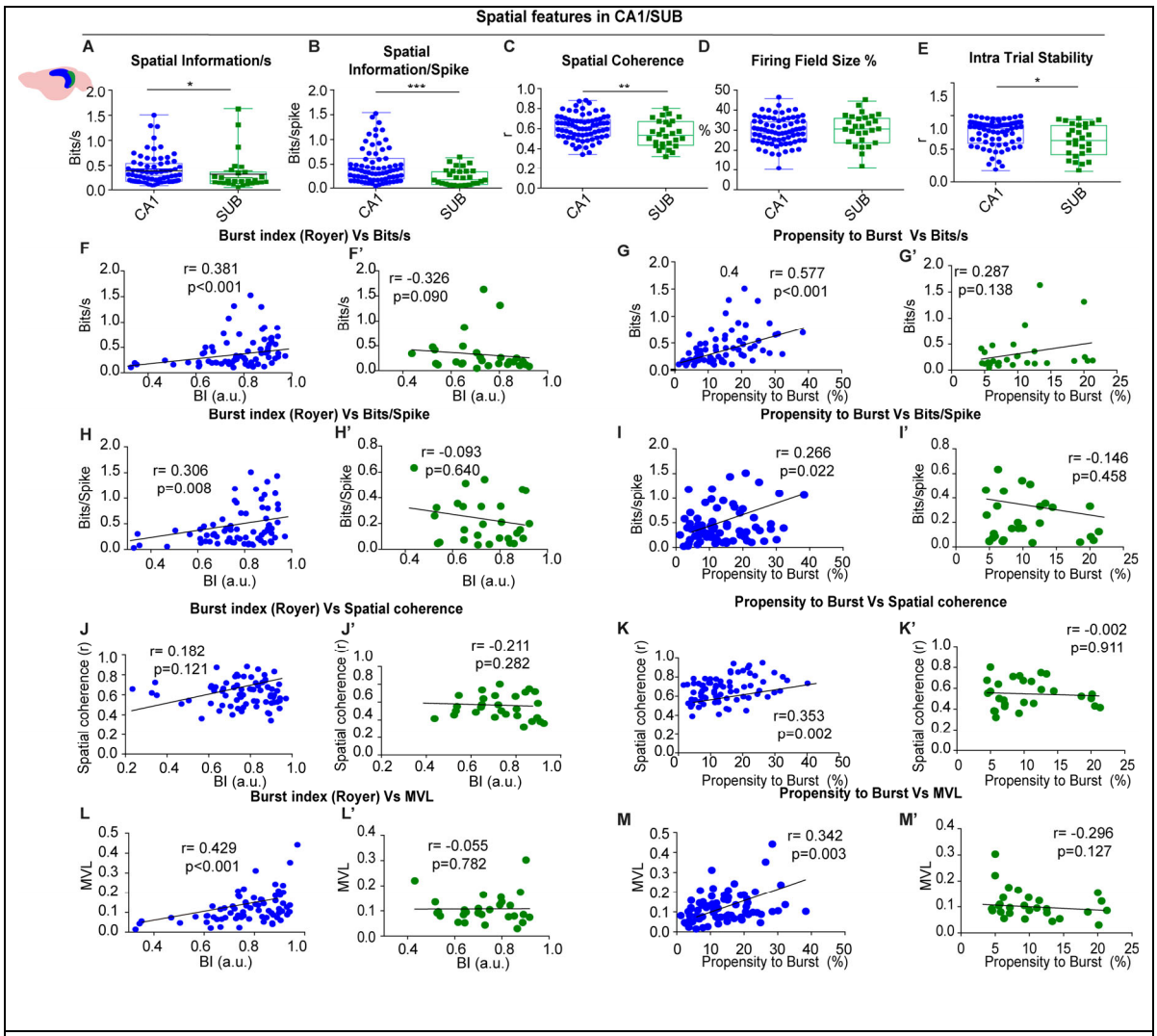

Figure 4. Spatial features in CA1 vs SUB (A–E) Group comparisons: spatial information per second, spatial information per spike, spatial coherence, firing-field size, and intra-trial stability and intra-trial stability were higher in CA1 (F–M′) Correlations between burst index or propensity to burst and spatial metrics (bits/s, bits/spike, coherence, MVL) for CA1 (blue) and SUB (green).

Spatial modulation of SUB units in the proximal region was not determined by bursting activity.

The spatial information is closely related to the electrophysiological characteristics of hippocampal pyramidal neurons. Specifically, place cells are known to exhibit complex spikes, or bursting activity, which is characterized by the generation of trains of action potentials within an envelope of 15-20 ms. This bursting pattern is thought to enhance

389 the fidelity of spatial information across different brain regions (44). We investigated if
390 there was a specific relationship between bursting patterns and the spatial modulation in
391 the CA1/SUB axis.

392 We found that in CA1 bursting metrics correlated with spatial modulation (Fig. 4F–M).
393 The burst index (BI) correlated with information per second ($r = 0.381$, $p < 0.001$,
394 Spearman) and information per spike ($r = 0.306$, $p = 0.008$), showed a trend for spatial
395 coherence ($r = 0.182$, $p = 0.18$, Spearman), and was strongly related to theta locking
396 (MVL; $r = 0.429$, $p < 0.001$, Spearman). The propensity to burst (PrtB) showed a similar
397 pattern: bits/s ($r = 0.577$, $p < 0.001$), bits/spike ($r = 0.266$, $p = 0.022$, Spearman), spatial
398 coherence ($r = 0.353$, $p = 0.002$, Spearman), and MVL ($r = 0.342$, $p = 0.003$, Spearman).
399 These relationships indicate that stronger bursting is associated with stronger spatial
400 coding and tighter theta–phase locking in CA1. Remarkably, we observed no correlation
401 between bursting properties and spatial modulation in SUB-recorded units, (Fig.4F'- M')
402 (BI vs bits per second, $r=-0.326$, $p=0.09$; BI vs bits per spike $r= -0.093$, $p=0.640$; BI vs
403 spatial coherence, $r= -0.211$, $p=0.282$; BI vs mean vector length, $r= -0.055$, $p=0.782$,
404 Spearman). A similar pattern was observed when we compared the bursting index with
405 the spatial modulation (PrtB vs bits per second, $r= 0.287$, $p=0.138$; PrtB vs bits per spike
406 $r= -0.146$, $p=0.458$; PrtB vs spatial coherence, $r= -0.002$, $p=0.991$; PrtB vs mean vector
407 length, $r= -0.296$, $p=0.127$, Spearman).

408 This indicates that CA1 neurons with a higher tendency to burst exhibited greater spatial
409 modulation, whereas in SUB-recorded neurons, bursting activity did not predict spatial
410 modulation, whether periodic or not.

411 Multisite Recordings

412 To validate and extend the tetrode findings, we implanted two additional mice with 64-
413 channel silicon probes targeting dorsal subiculum (see Fig 5A). Data were sorted with
414 KiloSort2 and manually curated in Phy2; cell-type labels were assigned with

CellExplorer (Petersen et al., 2021; see Methods). We isolated 196 with clear refractory periods: pyramidal neurons (PYR), *n* = 142; narrow-waveform interneurons (NW), *n* = 35; and wide-waveform interneurons (WW), *n* = 15, (see Fig 5B). Four units were deemed unclassified.

Spatial modulation

A unit was classified as spatially modulated (SM) if its rate-map spatial coherence exceeded the 95th percentile of a 1,000-iteration time-shift shuffle (See Methods). In total, 67/196 units (34.2%) met this criterion. Unless noted otherwise, the analyses below are restricted to pyramidal neurons.

Firing rate was higher in SM than in non-spatially modulated (NSM) PYR (Frequency 3.672 ± 0.347 Hz vs 2.585 ± 0.173 Hz; U = 4967, p = 0.0065; Mann–Whitney; Fig. 5C). By contrast, burst metrics—propensity to burst (PrtB) and burst index (BI)—and theta phase preference/locking did not differ between SM and NSM (PrtB: 2.441 ± 0.399 vs 12.389 ± 0.377; U = 5545, p = 0.849; Mann–Whitney Fig. 5D; BI: 2.286 ± 0.174 vs 2.081 ± 0.159; U = 5251, p = 0.139; Mann–Whitney, Fig. 5E); Theta phase (mean ± circSD, 3.443 ± 1.086 vs. 3.424 ± 0.978, Watson–Williams test: F(1) = 0.007, *p* = 0.935; Theta MVL: 0.114 ± 0.008 vs. 0.120 ± 0.006, U test: U = 4879, *p* = 0.524 Mann–Whitney, Figure F). As expected, SM units showed greater spatial information and within-session (intra-trial) stability than NSM (bits/spike: 0.145 ± 0.017 vs 0.062 ± 0.012, *U* = 4469, *p* < 0.0001; stability: 0.672 ± 0.025 vs 0.329 ± 0.025, *U* = 3877, *p* < 0.0001; Fig. 5G–H).

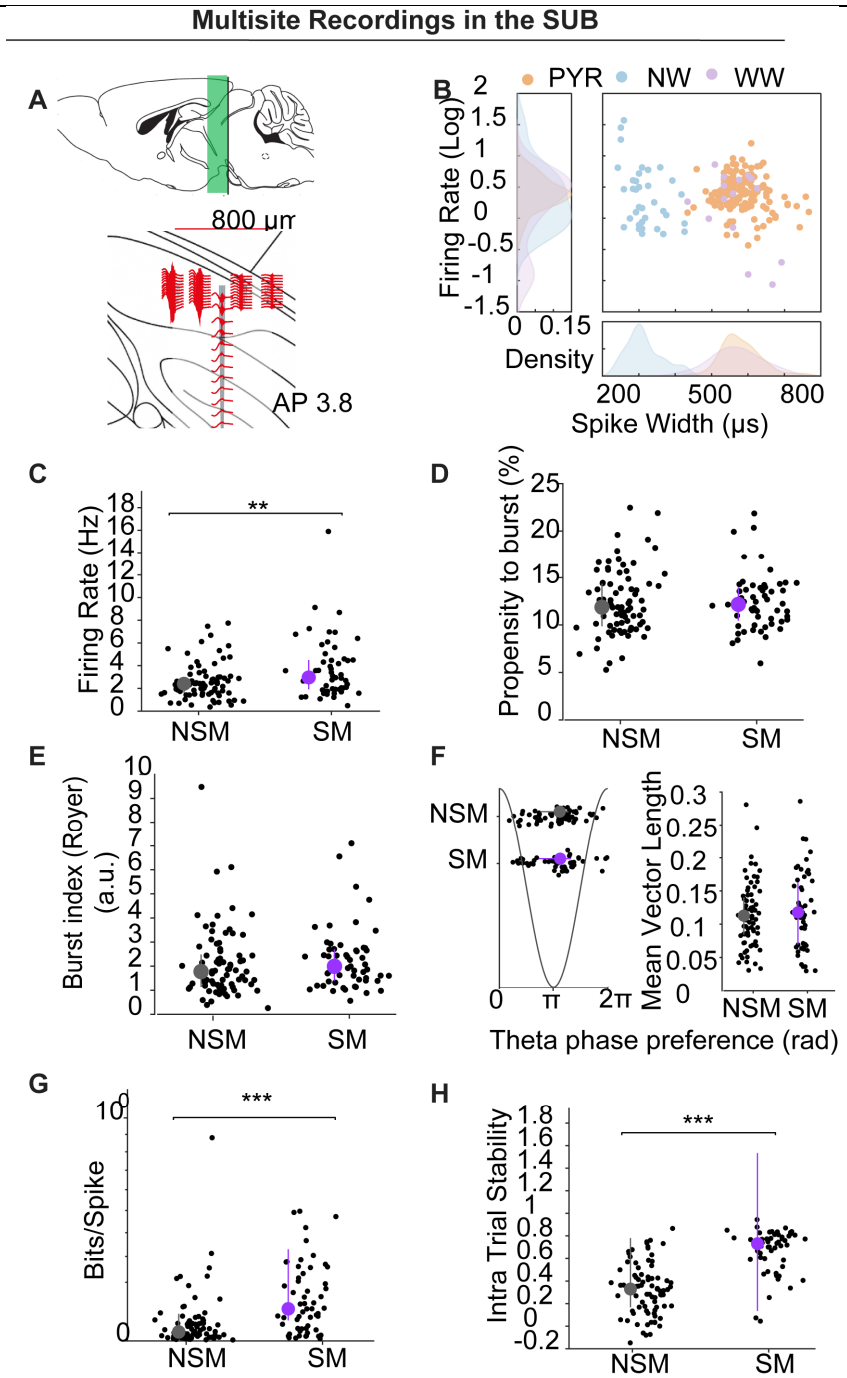

Figure 5. Multisite silicon-probe recordings in subiculum. (A) Schematic of probe geometry and dorsoventral span (~800 µm) targeting dorsal SUB (AP −3.8). (B) Cell-type classification by spike width and firing rate: pyramidal (PYR, orange), narrow-waveform interneurons (NW, blue), wide-waveform interneurons (WW, purple); density plots shown at margins. (C–H) Comparisons for firing rate (C), propensity to burst (D), burst index (E), theta phase preference/locking (F), spatial information (bits/spike) (G), and intra-trial stability (H) between NSM and SM pyramidal neurons. SM fired faster, had higher bits/spike and spatial stability with no differences in PrtB, BI, or theta metrics.

436 **Incidence of periodic cells and other spatial classes in multisite recordings**

437 In the probe cohort, 7/67 SM units (10.4%) met our a priori grid/periodicity criteria (four
438 and three cells in the two animals, respectively; Fig. 6A–C). Five of these were PYR
439 and two were NW interneurons (Fig. 6C). This incidence closely matches the tetrode
440 dataset (4/28 = 14.3%), under identical detection and shuffling thresholds, indicating
441 that periodic firing in mouse subiculum replicates across animals and recording
442 methods. We also identified **place cells (PC)** 36/67 (53,7%), **boundary-vector cells**
443 **(BVC)** 19/67 (28.4%), and **corner cells (CC)** 5/67 (7.5%) (Fig. 6D to 6F).

444 We next investigated potential difference across neuron types in multiple parameters,
445 for this analysis we included all types of neurons, with independence of its
446 electrophysiological type (Fig 7A–D). We found that spatial information per second was
447 higher in PC, BVC, and CC than in NSM (NSM 0.080 ± 0.011; PC 0.449 ± 0.046; BVC
448 0.497 ± 0.092; CC 0.322 ± 0.099; GC 0.226 ± 0.094; $\chi^2_{(4)} = 96.523$, $p < 0.0001$,
449 Kruskal–Wallis, Post-hoc (Dunn–Holm): PC > NSM (adjusted $p < 0.0001$), BVC > NSM
450 (adjusted $p < 0.0001$), CC > NSM (adjusted $p = 0.035$). Spatial information per spike
451 also differed among classes: NSM 0.052 ± 0.009; PC 0.156 ± 0.021; BVC 0.121 ±
452 0.029; CC 0.131 ± 0.061; GC 0.047 ± 0.022; $\chi^2_{(4)} = 42.985$, $p < 0.0001$, Kruskal–Wallis.
453 Post-hoc: PC > NSM (adjusted $p < 0.0001$), BVC > NSM (adjusted $p = 0.004$), PC >
454 GC (adjusted $p = 0.031$). Spatial coherence was higher for all spatial classes when
455 compare with NSM NSM 0.095 ± 0.008; PC 0.392 ± 0.021; BVC 0.441 ± 0.033; CC
456 0.369 ± 0.027; GC 0.308 ± 0.047; $\chi^2(4) = 116.918$, $p < 0.0001$; Kruskal-Wallis test.
457 Post-hoc: PC > NSM (adjusted $p < 0.0001$), BVC > NSM (adjusted $p < 0.0001$), CC >
458 NSM (adjusted $p = 0.003$), GD > NSM (adjusted $p = 0.005$).

459 We also verified that there were no significant differences in intra-trial spatial stability
460 between spatial types. On the other hand, they presented higher spatial stability than
461 non-spatially modulated neurons, although this effect was significant only for PC and

462 BVC (NSM r = 0.3199 ± 0.02; PC r = 0.68 ± 0.02; BVC r = 0.74 ± 0.03; CC r = 0.58 ±
463 0.14; GC r = 0.56 ± 0.07; $\chi^2_{(4)} = 84.93$, $p > 0.0001$, Kruskal–Wallis; Post-hoc PC > NSM
464 (adjusted $p < 0.0001$), BVC > NSM (adjusted $p < 0.0001$); CC vs NSM (adjusted $p =$
465 0.161); GC vs NSM (adjusted $p = 0.250$). Spatial cell types occurred throughout the
466 sampled proximodistal span (Fig. 7E).

467

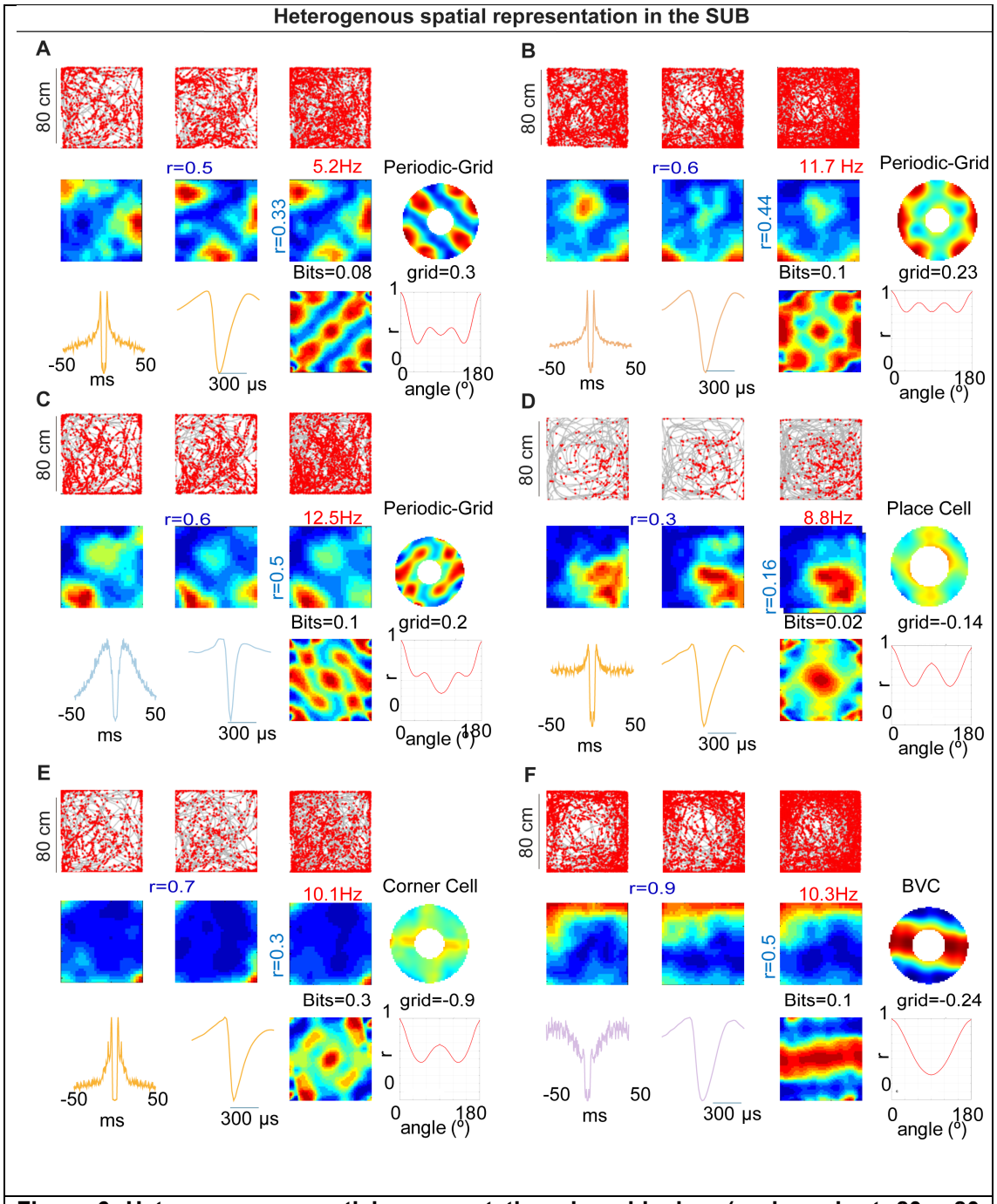

Figure 6. Heterogeneous spatial representations in subiculum (probe cohort, 80 × 80 cm). (A–C) Examples of periodic/grid-like neurons: trajectories with spikes, rate maps across time segments, spatial autocorrelograms, periodicity summaries (polar/orientation energy), and spike waveforms/ISI. (D) Example place cell. (E) Example corner cell with high corner-score field. (F) Example boundary-vector cell (BVC). For each neuron, grid score/periodicity measures and bits values are indicated on the panels. Across the cohort, spatial classes (PC, BVC, CC, GC, NSM) were distributed along the proximodistal axis.

Proximodistal axis spatial stability and bursting–spatial coupling

We investigated if there were differences in the intratrial spatial stability across the proximodistal axis. For this analysis we included all spatially modulated neurons with independence of their electrophysiological profile. We found no significant differences in these parameters (1.8 mm: 0.6920 ± 0.0426; 2.0 mm: 0.6383 ± 0.0451; 2.2 mm: 0.7397 ± 0.0345; 2.4 mm: 0.6988 ± 0.0375 $\chi^2(3) = 2.148$, $p = 0.542$, Kruskal–Wallis). Similar results were obtained for only pyramidal neurons, (data not shown).

In the tetrode dataset—which predominantly sampled proximal dorsal subiculum—burst metrics (BI, PrtB) did not correlate with spatial information. Given the known proximal→distal gradient in bursting propensity, we re-examined this in the probe dataset, which sampled ~800 µm along the proximodistal axis (Fig. 7G–H). Considering spatially modulated (pyramidal only) , bits/spike correlated positively with burst propensity in the most distal bin (ML 1.8: $r = 0.66$, $p = 0.027$), but not in more proximal bins (ML 2.0: $r = 0.21$, $p = 0.370$; ML 2.2: $r = 0.42$, $p = 0.579$; ML 2.4: $r = 0.20$, $p = 0.390$) (Fig. 7).

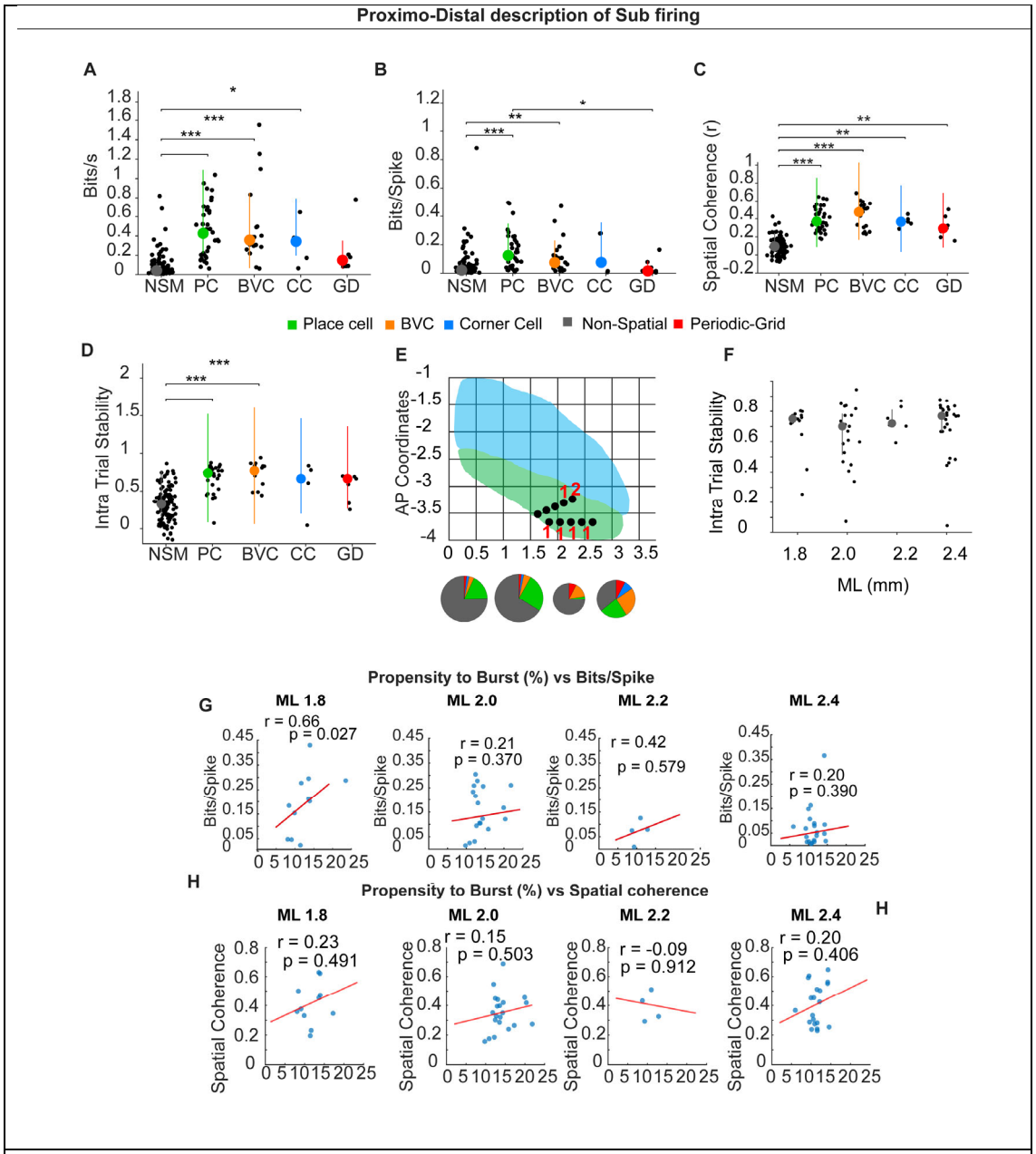

Figure 7. Different spatial types in the sub and Proximo–distal description of subicular firing. (A–D) Summary of spatial metrics across cell classes: NSM (non-spatial), PC (place cell), BVC (boundary-vector cell), CC (corner cell), and GD (grid/periodic). (E) Schematic of dorsal subiculum showing mediolateral (ML) and anteroposterior (AP) CA1 (blue) SUB (green). Black dots indicate recording sites; pie charts show cell-type composition within each ML bin representing numbers giving in the result text. (F). Intratrial stability across the proximo-distal axis. (G–H) Correlations (spatially modulated pyramidal neurons only) between propensity to burst (%) and spatial information (bits/spike) (F) or spatial coherence(G) computed within ML bins (1.8, 2.0, 2.2, 2.4 mm). Lines show least-squares fit; r and p are Pearson values. A significant positive relation appears distally (ML 1.8: r = 0.66, p = 0.027); other anatomical locations show no significant correlation.

493

Discussion

We provide the first evidence in mice that subicular pyramidal neurons exhibit grid-like/spatially periodic firing, using two independent technologies, custom tetrodes and high-density linear silicon probes. In the probe cohort, 7/67 spatially modulated cells (10.4%) met our grid/periodicity criteria (5 pyramidal, 2 interneurons), an incidence that closely matched the tetrode dataset (4/28 = 14.3%), indicating robustness and replicability across methods. Unit isolation met established sorting-quality benchmarks (23,27,45), and isolation quality did not differ between CA1 and SUB. Finally, spike waveforms and firing statistics were consistent with pyramidal neurons and inconsistent with putative axonal recordings (46).

Multisite (silicon-probe) recordings yielded higher unit counts and broader proximodistal coverage within dorsal SUB, enabling identification of multiple spatial classes—place cells, boundary-vector cells, and corner cells—all present across the proximodistal axis, and to understand better how bursting and firing rate might contribute to spatial information transmission.

SUB spatial representation is different to CA1

We observed that place cells in the CA1 showed higher spatial resolution as compared to SUB cells. This apparent lower spatial modulation of SUB neurons is related to their higher firing rate. Such augmented activity seems to serve as a mechanism to improve information routing from hippocampal formation to other brain regions, (47).

In the tetrode dataset, SUB neurons tended to fire near the center/peak of the theta cycle, which contrasts with prior reports showing a bias toward the descending phase and earlier than CA1 (47). This discrepancy may reflect recording location across the deep–superficial axis sampling. Consistent with this interpretation, the multisite probe recordings, which provide better laminar localization, revealed a phase preference like

519 the published pattern (47). Thus, the apparent mismatch in the tetrode data likely stems
520 from limited control over laminar position.

521 Proximodistal organization in the Subiculum

522 Inputs to the SUB are topographically organized, this way the proximal region of the SUB
523 receives information about inputs from LEC, known to be involved in the temporal coding
524 of episodes (48), while more distal regions integrate inputs from the MEC involved in
525 spatial coding (37), see O' Mara et all for a comprehensive review (49,50). In addition,
526 there is proximodistal gradient of burstiness, from lower in the proximal to higher in the
527 distal SUB, that might indicate a segregation of functions (51).

528 Our multisite recordings show that the dorsal subiculum hosts a diverse ensemble of
529 spatial codes rather than a single canonical type. Within the same animals we observed
530 place cells, boundary-vector cells (BVCs) that anchor firing to the geometry of nearby
531 boundaries, corner cells (CCs) with fields concentrated near vertices, and a subset of
532 neurons with spatially periodic (grid-like) activity. Importantly, these classes were
533 distributed along the proximodistal axis, rather than confined to a mediolateral specific
534 coordinate, indicating that geometric and periodic representations are features of
535 subicular circuitry. This heterogeneity suggests that SUB integrates inputs from CA1 and
536 entorhinal cortices to form complementary codes—spatial, boundary-anchored
537 (BVC/CC) and periodic tiling—that can support navigation and context generalization
538 across environments.

539 The presence of these codes across the proximodistal extent also implies parallel output
540 channels (49,50) from SUB to downstream cortico-subcortical targets, enabling these
541 different signals to be differentially routed rather than relying on a single encoding
542 scheme. This could be critical for the involvement of the sub in different cognitive
543 processes. In this sense, SUB neurons seem capable of maintaining active information
544 during the inter-trial in a working memory task (52). Such sustained or modulatory activity

545 could help signal the temporal structure of episodes, with distinct proximal–distal inputs
546 contributing to the organization of different information streams.

547 In our proximal SUB, tetrode recordings, spatial stability was lower than in CA1,
548 consistent with stronger LEC influence. However, in the multisite dataset we found no
549 significant proximodistal differences in intra-trial stability, suggesting that stability per se
550 is relatively uniform along the axis as well as also across different spatial cell types (
551 BVC/CC vs periodic).

552 It is relevant to mention that unlike CA1, where bursting often correlates with spatial
553 information and is thought to enhance synaptic reliability, tetrode recordings in the
554 subiculum did not show a uniform burst–spatial coupling. However, our multisite
555 recorded data resolved this discrepancy: burst propensity correlates with spatial
556 information only at more distal recording sites, whereas proximal SUB shows no such
557 relationship. This proximodistal dissociation suggests two coding regimes within SUB.
558 Proximally, spatial information is supported chiefly by elevated firing rates—a strategy
559 that can improve signal-to-noise and downstream reliability through temporal averaging
560 and redundant spiking. Distally, bursting contributes additional coding power beyond rate
561 aligning distal SUB more closely with CA1-like burst–information coupling. Given the
562 known gradients in intrinsic excitability, burst propensity, and projection targets along
563 SUB (51), these results are consistent with a functional multiplexing: rate-dominated
564 coding proximally and burst-augmented coding distally. Such organization could tailor
565 information transfer to distinct downstream circuits, with bursts selectively engaging
566 synapses or targets that are burst-sensitive, while higher rates maintain robust
567 throughput where bursts are less impactful.

568 The role of periodic firing in the SUB in spatial cognition

569 Speed and direction of movement are critical for path integration, and both inputs have
570 been proposed as essential for grid cells. This could be provided by GC ensembles (53).

571 From a mechanistic perspective, the computation of speed may rely on theta oscillations,
572 which are strongly correlated with velocity, as well as on speed cells (54–58). Moreover,
573 the direction of movement is of great relevance (59). This directional input may be
574 provided by axis cells described in the SUB (60). Complementary to these inputs, the
575 speed and directional signals could also be shaped by periodic cells in the MEC, pre-
576 parasubiculum and SUB units reported here (60,61). The redundancy of different speeds
577 and direction inputs might provide a more robust spatial integration for the navigation
578 across different conditions, for example across light-dark transitions.

579 Our new evidence of spatially periodic cells suggests that the SUB may contribute to
580 generating spatial representations by supporting periodic cells and GC in the pre-
581 parasubiculum and MEC. This is supported by anatomical data that confirms the strong
582 afferences sent by the SUB to the pre- and parasubiculum and the deep layers of the
583 MEC (16,62). Additionally, the SUB might provide input from boundary vector cells (BVC)
584 and periodic neurons to hippocampal place cells through its back projection to the CA1
585 area (63). In this way, circuits involving SUB-MEC, SUB-CA1, might support the
586 transformation of the grid produced by alterations of the geometry of space (64). Finally,
587 SUB spatial representation appears to depend on thalamic inputs and might meditate
588 changes in GC due to thalamic lesions also known to be relevant for GC in MEC (65).

589 In addition, two interneurons also met our grid/periodicity criteria, indicating that inhibition
590 can participate directly in spatially structured coding. This is consistent with recent
591 publication (25) demonstrating a cooperative role for interneurons in shaping spatial
592 representations.

593 Data limitation and context of the results

594 One limitation of the tetrode cohort was the small N, with grid-like firing observed in two
595 mice. Nevertheless, those units were stable across sessions and met stringent isolation
596 criteria (refractory-period violations and cluster-overlap probability). In one implant,

histology was incomplete, and the tetrode tip was not unambiguously visualized; depth was inferred from robust ripple activity, raising the possibility of partial sampling of adjacent regions (e.g., presubiculum), where ripples also occur (66). However, we obtained only one neurons from this implant. To address these concerns, we added an independent multisite probe cohort that provided higher yield and proximodistal coverage. In this dataset, 7/67 spatially modulated units (10.4%) met our priori periodic/grid criteria (5 pyramidal, 2 interneurons), an incidence that closely matched the tetrode dataset (4/28 = 14.3%) under identical analysis and shuffle thresholds. The replication across technologies and animals, together with consistent quality criteria and cell-type classification, substantially mitigates the small-sample caveat and supports the conclusion that periodic firing is a reproducible feature of mouse subiculum.

Conclusion

Here we present evidence of spatial periodic firing in the SUB. However, their response to complex spatial manipulation or their relationship with BVC, GC and place need to be determined. The SUB is of great relevance for the integration of the spatial code, episodic memory and dimensions related to the ongoing tasks. Further work should aim to investigate the role of the SUB in memory consolidation and spatial coding and in other cognitive processes.

Author Contributions:

JRBM designed the experiments. JRBM and PA, GR, GC, MS developed experiments, and implemented the analysis toolbox. FJMP and ME contributed to the implementation of the analysis and discussed the results. AF, VB and LM supported the project providing resources for its development and discussed the results. JBRM wrote the paper, and the manuscript was further reviewed, and data discussed by JRBM, PA, AF, and RS.

Acknowledgments

We would like to thank Liset Menendez de la Prida and Professor for her comments on this manuscript and their unconditional support for our work. Moreover, we want to thank Jim Donnett (Axona LTD) who was always available to help us with his technical support.

Funding: This project was supported by the Spanish State Research Agency, “Ministerio de Ciencia, Innovación y Universidades” (RTI2018-097474-A-100) obtained by JRBM, as well as by the UCHCEU (“Programa de Consolidación de Indicadores, AYUDAS PUENTE, Ayudas a grupos consolidados (GIR), GIR23/11.).

PA was funded by the UCHCEU-Banco de Santander fellowship.

VB was supported by grants from the European Research Council (309633) and the Spanish State Research Agency (PGC2018-102172-B-I00, as well as through the “Severo Ochoa" Programme for Centers of Excellence in R&D, ref. SEV-2017-0723).

The funders had no role in study design, data collection and analysis, decision to publish, or preparation of the manuscript.

References

1. O'Keefe J, Dostrovsky J. The hippocampus as a spatial map. Preliminary evidence from unit activity in the freely-moving rat. Brain Res [Internet]. 1971 Nov 12 [cited 2021 Dec 9];34(1):171–5. Available from: https://pubmed.ncbi.nlm.nih.gov/5124915/

2. Hafting T, Fyhn M, Molden S, Moser MB, Moser EI. Microstructure of a spatial map in the entorhinal cortex. Nature. 2005 Aug 11;436(7052):801–6.

3. Fyhn M, Hafting T, Witter MP, Moser EI, Moser MB. Grid cells in mice. Hippocampus. 2008 Dec;18(12):1230–8.

4. Taube JS, Muller RU, Ranck JB. Head-direction cells recorded from the postsubiculum in freely moving rats. I. Description and quantitative analysis. J Neurosci. 1990;10(2):420–35.

5. Lever C, Burton S, Jeewajee A, O'Keefe J, Burgess N. Boundary Vector Cells in the Subiculum of the Hippocampal Formation. The Journal of Neuroscience. 2009 Aug 8;29(31):9771.

6. Solstad T, Boccara CN, Kropff E, Moser MB, Moser EI. Representation of geometric borders in the entorhinal cortex. Science. 2008 Dec 19;322(5909):1865–8.

7. Sharp PE, Green C. Spatial correlates of firing patterns of single cells in the subiculum of the freely moving rat. J Neurosci. 1994;14(4):2339–56.

8. Brotons-Mas JR, Schaffelhofer S, Guger C, O'Mara SM, Sanchez-Vives M V. Heterogeneous spatial representation by different subpopulations of neurons in the subiculum. Neuroscience. 2017 Feb 20;343:174–89.

9. McNaughton BL, Battaglia FP, Jensen O, Moser EI, Moser MB. Path integration and the neural basis of the "cognitive map." Nat Rev Neurosci [Internet]. 2006 Aug [cited 2024 Nov 20];7(8):663–78. Available from: https://pubmed.ncbi.nlm.nih.gov/16858394/

10. Hartley T, Burgess N, Lever C, Cacucci F, O'keefe J. Modeling Place Fields in Terms of the Cortical Inputs to the Hippocampus. 2000;

11. O'Keefe J, Burgess N. Dual phase and rate coding in hippocampal place cells: Theoretical significance and relationship to entorhinal grid cells. Hippocampus. 2005;15(7):853–66.

12. Wills TJ, Cacucci F, Burgess N, O'Keefe J. Development of the hippocampal cognitive map in preweanling rats. Science (1979). 2010 Jun 18;328(5985):1573–6.

13. Langston RF, Ainge JA, Couey JJ, Canto CB, Bjerknes TL, Witter MP, et al. Development of the spatial representation system in the rat. Science (1979). 2010 Jun 18;328(5985):1576–80.

14. Morris G, Derdikman D. The chicken and egg problem of grid cells and place cells. Trends Cogn Sci [Internet]. 2023 Feb 1 [cited 2024 Jun 13];27(2):125–38. Available from: https://pubmed.ncbi.nlm.nih.gov/36437188/

15. Aggleton JP, Christiansen K. The subiculum: The heart of the extended hippocampal system. Prog Brain Res. 2015;219:65–82.

16. O'Mara SM, Sanchez-Vives M V., Brotons-Mas JR, O'Hare E. Roles for the subiculum in spatial information processing, memory, motivation and the temporal control of behaviour. Prog Neuropsychopharmacol Biol Psychiatry. 2009 Aug 1;33(5):782–90.

17. Sharp PE. Subicular cells generate similar spatial firing patterns in two geometrically and visually distinctive environments: Comparison with hippocampal place cells. Behavioural Brain Research. 1997 Apr;85(1):71–92.

18. Brotons-Mas JR, Montejo N, O'Mara SM, Sanchez-Vives M V. Stability of subicular place fields across multiple light and dark transitions. European Journal of Neuroscience. 2010 Aug;32(4):648–58.

19. Barnes CA, McNaughton BL, Mizumori SJY, Leonard BW, Lin LH. Chapter 21 Chapter Comparison of spatial and temporal characteristics of neuronal activity in sequential stages of hippocampal processing. Prog Brain Res. 1990 Jan 1;83(C):287–300.

20. Ledergerber D, Battistin C, Blackstad JS, Gardner RJ, Witter MP, Moser MB, et al. Task-dependent mixed selectivity in the subiculum. Cell Rep. 2021 May 25;35(8).

21. Eller J, Zarnadze S, Bäuerle P, Dugladze T, Gloveli T. Cell Type-Specific Separation of Subicular Principal Neurons during Network Activities. 2015;

22. Jarsky T, Mady R, Kennedy B, Spruston N. Distribution of Bursting Neurons in the CA1 Region and the Subiculum of the Rat Hippocampus. J Comp Neurol. 2008;506:535–47.

23. Krupic J, Burgess N, O'Keefe J. Neural representations of location composed of spatially periodic bands. Science (1979) [Internet]. 2012 Aug 17 [cited 2021 May 31];337(6096):853–7. Available from: https://pubmed.ncbi.nlm.nih.gov/22904012/

24. Del Pino I, Brotons-Mas JR, Marques-Smith A, Marighetto A, Frick A, Marín O, et al. Abnormal wiring of CCK+ basket cells disrupts spatial information coding. Nat Neurosci. 2017 Jun 1;20(6):784–92.

25. Valero M, Abad-Perez P, Gallardo A, Picco M, García-Hernandez R, Brotons J, et al. Cooperative actions of interneuron families support the hippocampal spatial code. Science (1979) [Internet]. 2025 Sep 4 [cited 2025 Oct 1];389(6764):eadv5638. Available from: /doi/pdf/10.1126/science.adv5638?download=true

26. Del Pino I, García-Frigola C, Dehorter N, Brotons-Mas JR, Alvarez-Salvado E, MartínezdeLagrán M, et al. Erbb4 Deletion from Fast-Spiking Interneurons Causes Schizophrenia-like Phenotypes. Neuron. 2013 Sep 18;79(6):1152–68.

27. Hill DN, Mehta SB, Kleinfeld D. Quality Metrics to Accompany Spike Sorting of Extracellular Signals. 2011;

28. Royer S, Sirota A, Patel J, Buzsáki G. Distinct representations and theta dynamics in dorsal and ventral hippocampus. Journal of Neuroscience. 2010 Feb 3;30(5):1777–87.

29. Staff NP, Jung HY, Thiagarajan T, Yao M, Spruston N. Resting and active properties of pyramidal neurons in subiculum and CA1 of rat hippocampus. J Neurophysiol [Internet]. 2000 [cited 2024 Apr 20];84(5):2398–408. Available from: https://journals.physiology.org/doi/10.1152/jn.2000.84.5.2398

30. Valero M, Zutshi I, Yoon E, Buzsáki G. Probing subthreshold dynamics of hippocampal neurons by pulsed optogenetics. Science (1979) [Internet]. 2022 [cited 2022 Nov 8];375:570–4. Available from: https://www.science.org

31. Berens P. CircStat: A MATLAB Toolbox for Circular Statistics. J Stat Softw [Internet]. 2009 Sep 23 [cited 2025 Oct 1];31(10):1–21. Available from: https://www.jstatsoft.org/index.php/jss/article/view/v031i10

32. Pérez PA, Molina-Paya F, Falco A, Otero LM, Valero M, Borrell V, et al. ELECTROPHYSIOLOGICAL AND NETWORK PROPERTIES OF SPATIAL-RELATED NEURONS IN THE SUBICULUM OF MICE. IBRO Neurosci Rep [Internet]. 2023 Oct 1 [cited 2025 Jan 28];15:S806–7. Available from: http://www.ibroneuroreports.org/article/S2667242123017293/fulltext

33. Markus EJ, Barnes CA, Bruce $, Mcnaughton L, Gladden VL, Skaggs WE. Spatial Information Content and Reliability of Hippocampal CA1 Neurons: Effects of Visual Input. HZPPOCAMPUS. 1994;4(4):410–21.

34. Muller RU, Kubie JL. The effects of changes in the environment on the spatial firing of hippocampal complex-spike cells. J Neurosci. 1987;7(7):1951–68.

35. Lever C, Burton S, Jeewajee A, O'Keefe J, Burgess N. Boundary Vector Cells in the Subiculum of the Hippocampal Formation. The Journal of Neuroscience [Internet]. 2009 Aug 8 [cited 2022 Oct 18];29(31):9771. Available from: /pmc/articles/PMC2736390/

36. Sun Y, Nitz DA, Xu X, Giocomo LM. Subicular neurons encode concave and convex geometries. Nature [Internet]. 2024 Mar 28 [cited 2025 Oct 1];627(8005):821–9. Available from: https://www.nature.com/articles/s41586-024-07139-z

37. Hafting T, Fyhn M, Molden S, Moser MB, Moser EI. Microstructure of a spatial map in the entorhinal cortex. Nature. 2005 Aug 11;436(7052):801–6.

38. Sargolini F, Fyhn M, Hafting T, McNaughton BL, Witter MP, Moser MB, et al. Conjunctive representation of position, direction, and velocity in entorhinal cortex. Science (1979) [Internet]. 2006 May 5 [cited 2024 Aug 19];312(5774):758–62. Available from: https://www.science.org/doi/10.1126/science.1125572

39. Muessig L, Ribeiro Rodrigues F, Bjerknes TL, Towse BW, Barry C, Burgess N, et al. Environment geometry alters subiculum boundary vector cell receptive fields in adulthood and early development. Nat Commun [Internet]. 2024 Dec 1 [cited 2025 Oct 1];15(1):1–17. Available from: https://www.nature.com/articles/s41467-024-45098-1

40. Mizuseki K, Kitanishi T. Oscillation-coordinated, noise-resistant information distribution via the subiculum. Curr Opin Neurobiol. 2022 Aug 1;75:102556.

41. Valero M, de la Prida LM. The hippocampus in depth: a sublayer-specific perspective of entorhinal–hippocampal function. Vol. 52, Current Opinion in Neurobiology. Elsevier Ltd; 2018. p. 107–14.

42. Oliva A, Fernández-Ruiz A, Buzsáki G, Berényi A. Spatial coding and physiological properties of hippocampal neurons in the Cornu Ammonis subregions. Hippocampus. 2016 Dec 1;26(12):1593–607.

43. Leutgeb S, Leutgeb JK, Barnes CA, Moser EI, McNaughton BL, Moser MB. Neuroscience: Independent codes for spatial and episodic memory in hippocampal neuronal ensembles. Science (1979). 2005 Jul 22;309(5734):619–23.

44. Simonnet J, Brecht M. Burst firing and spatial coding in subicular principal cells. Journal of Neuroscience. 2019 May 8;39(19):3651–62.

45. Navratilova Z, Godfrey KB, McNaughton BL. Grids from bands, or bands from grids? An examination of the effects of single unit contamination on grid cell firing fields. J Neurophysiol. 2016 Feb 19;115(2):992–1002.

46. Robbins AA, Fox SE, Holmes GL, Scott RC, Barry JM. Short duration waveforms recorded extracellularly from freely moving rats are representative of axonal activity. Front Neural Circuits [Internet]. 2013 [cited 2024 Aug 19];7:181. Available from: /pmc/articles/PMC3831546/

780 47. Kitanishi T, Umaba R, Mizuseki K. Robust information routing by dorsal
781 subiculum neurons. Sci Adv. 2021 Mar 1;7(11).

782 48. Tsao A, Sugar J, Lu L, Wang C, Knierim JJ, Moser MB, et al. Integrating time from
783 experience in the lateral entorhinal cortex. Nature. 2018 Sep 6;561(7721):57–62.

784 49. O'Mara SM, Commins S, Anderson M, Gigg J. The subiculum: A review of form,
785 physiology and function. Prog Neurobiol. 2001;64(2):129–55.

786 50. O'Mara SM, Sanchez-Vives M V., Brotons-Mas JR, O'Hare E. Roles for the
787 subiculum in spatial information processing, memory, motivation and the
788 temporal control of behaviour. Prog Neuropsychopharmacol Biol Psychiatry.
789 2009 Aug 1;33(5):782–90.

790 51. Cembrowski MS, Phillips MG, DiLisio SF, Shields BC, Winnubst J, Chandrashekar
791 J, et al. Dissociable Structural and Functional Hippocampal Outputs via Distinct
792 Subiculum Cell Classes. Cell. 2018 May 17;173(5):1280-1292.e18.

793 52. Deadwyler SA, Hampson RE. Differential but complementary mnemonic
794 functions of the hippocampus and subiculum. Neuron. 2004 May 13;42(3):465–
795 76.

796 53. Zutshi I, Leutgeb JK, Leutgeb S. Theta sequences of grid cell populations can
797 provide a movement-direction signal. Curr Opin Behav Sci. 2017 Oct 1;17:147–
798 54.

799 54. Kramis R, Vanderwolf CH, Bland BH. Two types of hippocampal rhythmical slow
800 activity in both the rabbit and the rat: Relations to behavior and effects of
801 atropine, diethyl ether, urethane, and pentobarbital. Exp Neurol. 1975 Oct
802 1;49(1):58–85.

803 55. Chen Z, Resnik E, McFarland JM, Sakmann B, Mehta MR. Speed Controls the
804 Amplitude and Timing of the Hippocampal Gamma Rhythm. PLoS One.
805 2011;6(6):e21408.

806 56. Long LL, Hinman JR, Chen CM, Escabi MA, Chrobak JJ. Theta dynamics in rat:
807 Speed and acceleration across the septotemporal axis. PLoS One. 2014 May
808 19;9(5).

809 57. Kropff E, Carmichael JE, Moser EI, Moser MB. Frequency of theta rhythm is
810 controlled by acceleration, but not speed, in running rats. Neuron. 2021 Mar
811 17;109(6):1029-1039.e8.

812 58. Abad-Perez P, Molina-Payá FJ, Martínez-Otero L, Borrell V, Redondo RL, Brotons-
813 Mas JR. Theta/gamma Co-modulation Disruption After NMDAr Blockade by MK-
814 801 Is Associated with Spatial Working Memory Deficits in Mice. Neuroscience.
815 2023 May 21;519:162–76.

59. Raudies F, Brandon MP, Chapman GW, Hasselmo ME. Head direction is coded more strongly than movement direction in a population of entorhinal neurons. Brain Res. 2015 Sep 24;1621:355–67.

60. Olson JM, Tongprasearth K, Nitz DA. Subiculum neurons map the current axis of travel. Nat Neurosci. 2017 Feb 1;20(2):170–2.

61. Jeewajee A, Barry C, O'Keefe J, Burgess N. Grid cells and theta as oscillatory interference: Electrophysiological data from freely moving rats. Hippocampus. 2008 Dec;18(12):1175–85.

62. O'Mara SM, Commins S, Anderson M, Gigg J. The subiculum: A review of form, physiology and function. Prog Neurobiol. 2001;64(2):129–55.

63. Xu X, Sun Y, Holmes TC, López AJ. Noncanonical connections between the subiculum and hippocampal CA1. J Comp Neurol. 2016 Dec 1;524(17):3666–73.

64. Krupic J, Bauza M, Burton S, Barry C, O'Keefe J. Grid cell symmetry is shaped by environmental geometry. Nature. 2015 Feb 12;518(7538):232–5.

65. Frost BE, Cafalchio M, Martin SK, Islam N, Aggleton JP, O'mara SM. Spatial Coding in the Subiculum Requires Anterior Thalamic Inputs. [cited 2020 Feb 19]; Available from: https://doi.org/10.1101/2020.01.31.928762

66. Chrobak JJ, Buzsáki G. High-Frequency Oscillations in the Output Networks of the Hippocampal–Entorhinal Axis of the Freely Behaving Rat. Journal of Neuroscience [Internet]. 1996 May 1 [cited 2024 Sep 9];16(9):3056–66. Available from: https://www.jneurosci.org/content/16/9/3056